Title
The Type I BMP Receptor ACVR1/ALK2 is Required for Chondrogenesis During Development

Journal
Journal of Bone and Mineral Research, 30(4)

ISSN
0884-0431

Authors
Rigueur, Diana
Brugger, Sean
Anbarchian, Teni
et al.

Publication Date
2015-04-01

DOI
10.1002/jbmr.2385

Peer reviewed

J Bone Miner Res. Author manuscript; available in PMC 2016 Apr 1.

Published in final edited form as:

J Bone Miner Res. 2015 Apr; 30(4): 733–741.

doi: 10.1002/jbmr.2385

PMCID: PMC4376569

NIHMSID: NIHMS637739

PMID: 25413979

The type I BMP receptor ACVR1/ALK2 is required for chondrogenesis during development

Diana Rigueur,[1] Sean Brugger,[2] Teni Anbarchian,[1,2] Jong Kil Kim,[1] Yoo Jin Lee,[2,3] and Karen Lyons[1,2,3]

Author information Copyright and License information Disclaimer

Introduction

Bone morphogenetic proteins (BMP) are crucial regulators of chondrogenesis. BMPs transduce their signals through three type I receptors: BMP receptor type 1A (BMPR1A, also known as ALK3), BMPR1B (ALK6), and activin receptor type 1A (ACVR1/ActR1/ALK2). BMPR1A and BMPR1B are structurally similar and bind BMPs (1). ACVR1 binds to a more diverse set of ligands, including TGFβs, activins, and multiple BMPs (2-4).

The majority of the vertebrate skeleton forms through endochondral ossification, and BMPs play essential roles at many steps in this process. BMP signaling is required to maintain expression of Sox9, a transcription factor essential for commitment to the chondrogenic fate (5,6), and for these cells to differentiate as chondrocytes and organize into a growth plate. The growth plate consists of zones of proliferating cells, followed by post-mitotic prehypertrophic and hypertrophic chondrocytes (7). BMP signaling is required to promote proliferation and differentiation (8-10). Growth plates form in mice deficient in *Bmpr1a* or *Bmpr1b*, but chondrogenesis is arrested at the condensation stage in mice lacking both receptors in cartilage (6,10,11). The function of ACVR1/ALK2 is not as well characterized. The ability of ACVR1 to promote chondrogenesis has been established *in vitro* (12,13). Its importance *in vivo* is demonstrated by the fact that fibrodysplasia ossificans progressiva (FOP), a rare disorder characterized by progressive ossification of connective tissue (14), is caused by an activating mutation in *Acvr1* (the gene that encodes ALK2) (15,16). Constitutively active ACVR1 can cause ectopic endochondral ossification (17). The activating mutant can also enhance chondrogenic commitment of progenitor cells and predispose

mesenchymal cells to an osteoblastic fate (18 {Culbert, 2014 #46}). However, FOP patients have only subtle developmental defects (14). Therefore, whether ACVR1 activity is required for normal chondrogenesis is unknown. Moreover, whether this receptor has unique functions in line with its unique ability to engage diverse TGFβ ligands is unknown. We generated mice lacking ACVR1 in cartilage to address these questions.

Materials and Methods

Generation of *Acvr1*^{CKO} and *Bmpr1a*^{CKO};*Acvr1*^{CKO}, and *Bmpr1b−/−*;*Acvr1*^{CKO} mice

Generation and genotyping of *Bmpr1b*, *Bmpr1a*, *Acvr1*, and *Col2-Cre* mice was described previously (11,19-21). To generate cartilage-specific *Acvr1* null mice, *Acvr1*$^{fx/+}$*;Col2-Cre* mice were intercrossed to generate *Acvr1*$^{fx/fx}$*;Col2-Cre* (*Acvr1*^{CKO}) mice. *Acvr1*$^{f+/-}$*;Bmpr1a* $^{fx/+;}$*Col2-Cre* mice were intercrossed to generate *Acvr1*^{CKO}*;Bmpr1a*^{CKO}*;*mice (referred to as *Acvr1/Bmpr1a*^{CKO}). An analogous scheme was used to generate *Acvr1*^{CKO}*;Bmpr1b−/−* mice. All procedures were approved by the Institutional Animal Care and Use Committee at UCLA (IACUC protocol number 95-018).

Skeletal preparation and histology

Skeletal preparations were performed as described (22). For histology, embryos were fixed in 4% paraformaldehyde, decalcified, and embedded in paraffin. Sections were stained with hematoxylin and eosin or alcian blue and nuclear fast red (23).

Immunohistochemistry

Primary antibodies were ACVR1/ALK2 (Sigma SAB1306388-40TST, 1:100), PCNA (Zymed, 13-3900), phospho-SMAD1/5 (Cell Signaling Technology), or p-p38 (Cell Signaling Technology, 9211 ,1:00). As a control for specificity, a second ACVR1 antibody (Abcam 155981, 1:100) was used for IHC; similar results were obtained (data not shown). Sections were quenched in 3% H_2O_2 in methanol, blocked with 0.5% blocking reagent (TSA Biotin System, Perkin Elmer, Waltham, MA, USA, NEL700A) in TBS (100 mM Tris pH 7.5, 150 mM NaCl), incubated with primary antibody overnight at 4° C, and then washed and incubated overnight at 4°C with Alexa-Fluor-488 or −555-conjugated rabbit secondary antibody (Invitrogen). Detection of antibody binding was performed using the TSA Biotin System according to the manufacture's instructions. Fluorescence detection was conducted using Streptavidin–AlexaFluor -488 or -555 (Invitrogen) secondary antibodies; sections were counterstained with DAPI (Invitrogen, D1306). Quantitation of pSmad1/5 and PCNA-positive cells was performed as described (24); at least three sections from 5 mice per genotype were examined by individuals blinded to genotype. Total cells (DAPI-positive) and the percentage of total cells (DAPI-positive cells that were also pSmad1/5-positive) were determined and statistical significance assessed using Students *t* test (24).

Western blot analysis

Primary chondrocytes were isolated from costal cartilage as described (25) and seeded at 1X 10^5 cells/well in 12-well plates. Cells were maintained in chondrogenic medium for 3 days. They were then washed twice with 1x PBS and treated with ACVR1/ALK2 shRNA lentivirus transmission particles (Sigma-Aldrich SHCLNV-NM_007394; TRCN0000361057) at an MOI of 10 in serum free medium for 24 hrs. Cells were then maintained in chondrogenic medium for 72 hrs. Cells were lysed in RIPA buffer supplemented with protease and phosphatase inhibitors as described (25). Whole cell lysates were run on 10% SDS-polyacrylamide gels and transferred onto PVDF membranes. The membranes were blocked with 5% milk in TBS-Tween (30 mM Tris pH 74, 300 mM NaCl, 0.2% Tween 20), incubated with primary antibody (ACVR1/ALK2, Sigma SAB1306388-40TST (1:100); Tubulin, Cell Signaling 2144 (1:2000)) for 1hr at

RT and then incubated with secondary antibody diluted in blocking buffer for 1 h at room temperature. Binding was detected using the ECL Plus kit (GE Healthcare).

X-ray and microCT analysis

X-ray analyses of adult mice were performed using a Faxitron as described (11). MicroCT analysis of neonates was performed as described (22).

Results

Expression of ACVR1/ALK2

We examined ACVR1 protein expression in the skeletal system from E10.5 through birth (P0). Western analysis revealed that the antibody employed in these studies detected a single band of the expected size of approximately 57 kD in primary chondrocytes; lentiviral shRNA against ACVR1 significantly reduced the detection of this band (Supplemental Fig. 1). The results are consistent with and extend previous *in situ* hybridization studies (12,26,27), which indicated diffuse expression of *Acvr1 (Alk2*) mRNA throughout the growth plate. In craniofacial elements, expression was detected beginning at E10.5 in mesenchyme (Supplemental Fig. 2A), and by E12.5, in condensing cartilage (Supplemental Fig. 2B). By E14.5, expression was seen in proliferating chondrocytes in the sphenoid and at lower levels in adjacent resting chondrocytes in the spheno-occipital synchondrosis (Supplemental Fig 2C). At E16.5, expression persisted in proliferating chondrocytes, and high levels of ACVR1 protein were seen in hypertrophic chondrocytes (Supplemental Fig. 2D,E). This expression persisted at P0 (data not shown).

ACVR1 protein was not strongly expressed in appendicular elements until a growth plate had formed. At E13.5, ACVR1 protein was detected in proliferating chondrocytes, and at higher levels in hypertrophic chondrocytes (Supplemental Fig. 2F). By E16.5, ACVR1 protein expression persisted in proliferating chondrocytes but was expressed at higher levels in hypertrophic chondrocytes (Supplemental Fig. 2G). This pattern persisted through P0 (data not shown).

The highest levels and earliest onset of ACVR1 protein expression were detected in axial elements. Expression was first seen at E11.5 in sclerotomal cells (Fig. 1A-D). Consistent with a previous report (28) ACVR1 protein was also expressed in the notochord at this stage (Fig. 1C,D). By E13.5, ACVR1 protein expression was strong in the nucleus pulposus. Expression could also be seen in proliferating chondrocytes in vertebral bodies (Fig. 1E,F). This pattern persisted at E15.5 (Fig. 1G). At P0, expression was strong in the nucleus pulposus, and persisted in the proliferating chondrocytes in cartilage endplates of vertebral bodies (Fig. 1H).

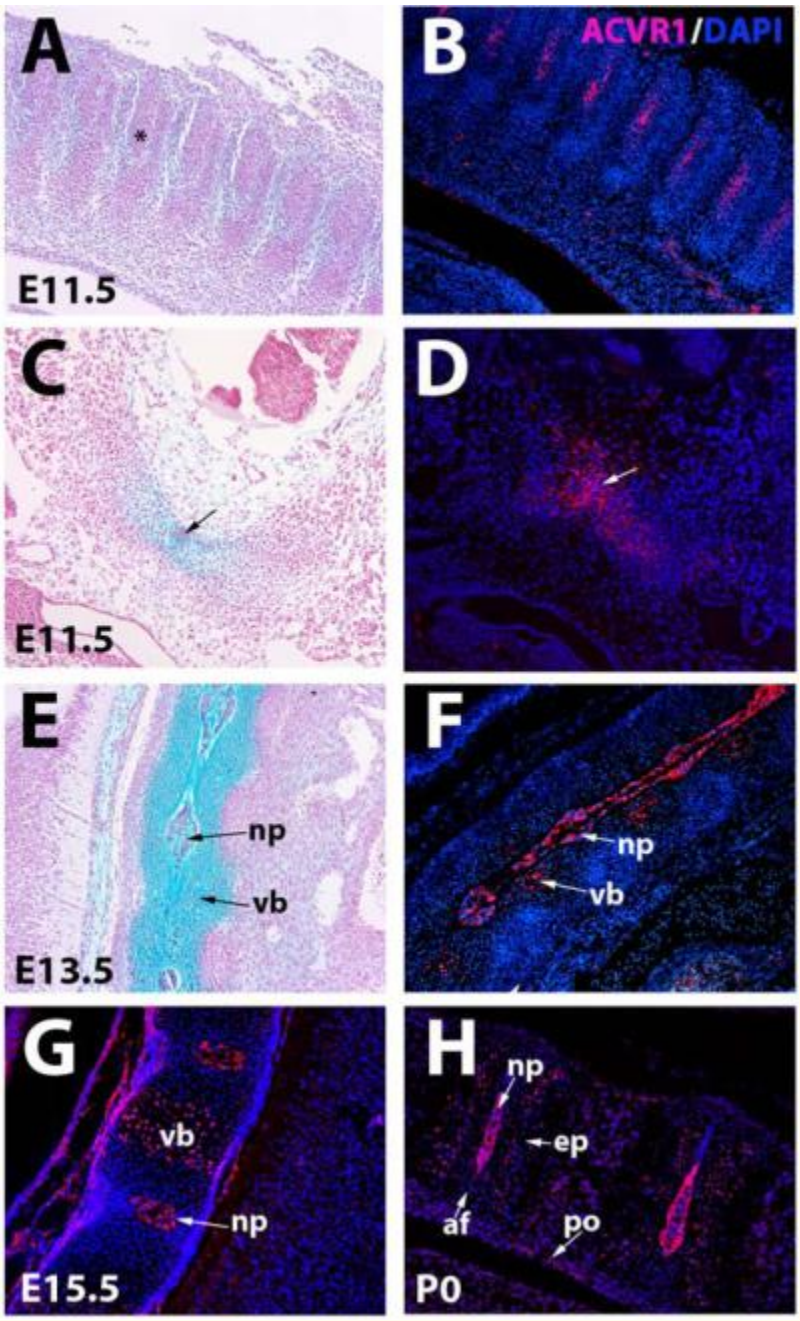

Figure 1
ACVR1/ALK2 protein expression in axial elements

A, C. and E are stained with alcian blue-nuclear fast red. B, D, F, G, H are immunofluorescent images counterstained with DAPI. A,B, E11.5 cervical region showing ACVR1/ALK2 protein is expressed in sclerotome (asterisk). C,D. E11.5 cervical region showing expression in precartilaginous mesenchyme (detected by alcian blue staining in C), and notochord (arrows). E,F, Sections through E13.5 cervical spine showing expression in nucleus pulposus and chondrocytes in the vertebrae. G, E15.5 cervical spine showing expression in nucleus pulposus and proliferating chondrocytes in vertebral bodies. H, P0 cervical spine showing expression in endplate cartilage and nucleus pulposus. Low levels of expression are present in the periosteum of the vertebrae. Af, annulus fibrosus; ep, endplate; np, nucleus pulposus; po, periosteum; vb, vertebral body.

While our studies of ACVR1 protein localization, indicating expression throughout midgestation stages in proliferating chondrocytes, notochord, and perichondrium are consistent with previous *in situ* studies (12,26,27) our finding of relatively higher levels of ACVR1 protein in hypertrophic chondrocytes would not be predicted from these studies. It is conceivable that ACVR1 protein produced in less mature

chondrocytes persists and accumulates on the surface of maturing chondrocytes. However, we cannot rule out the possibility of cross-reactivity with an unrelated antigen in the hypertrophic zone, as discussed further below.

Phenotype of mice lacking AVCR1/ALK2 in cartilage

We used a conditional allele of *Acvr1* (*Alk2)* (21) to investigate the function of ACVR1 in cartilage. To assess the efficiency of recombination and as a test of specificity of the ACVR1 antibody used to characterize ACVR1 expression, we performed IHC on *Acvr1*$^{fx/fx}$*;Col2a1-Cre* (hereafter referred to as *Acvr1*^{CKO}) growth plates (Supplemental Figure 3A,B). This analysis revealed that at least 80% of the proliferating chondrocytes had undergone efficient recombination (Supplemental Figure 3C). Immunoreactivity persisted in the nucleus pulposus as expected since this structure is not derived from *Col2a1-Cre* expressing cells. Within *Col2a1-Cre* expressing cells, immunoreactivity persisted in hypertrophic chondrocytes in mutants. As discussed above, we cannot rule out the possibility that this represents cross-reactivity of the antibodies we used. However, the strong reduction in ACVR1 protein observed in *Acvr1*^{CKO} vertebral chondrocytes argues that efficient recombination occurred and that the antibody used to detect ACVR1 protein displays reasonable specificity.

Acvr1^{CKO} mice were recovered in Mendelian ratios. No abnormalities were seen in heterozygotes. However, *Acvr1*^{CKO} neonates exhibited axial defects with 100% penetrance (n = 23). The cervical vertebral column was compressed, and cervical elements were thinner and broader than in WT littermates (Fig. 2A,B). Transverse views showed that the diameters of cervical vertebrae were enlarged in mutants (Fig. 2C-E'). The vertebral arches of C (cervical) 1 (Fig. 2C,C') and C2 (Fig. 2D,D') vertebrae were hypoplastic and failed to fuse. Transverse processes on C3 through C7 were incomplete (Fig. 2E,E', and data not shown), and the centra exhibited delayed ossification. Histological analyses did not reveal obvious defects in the sizes of condensations, or in chondrocyte differentiation in axial or appendicular elements at E13.5 (Supplemental Fig. 4), suggesting either a subtle defect, and/or later onset.

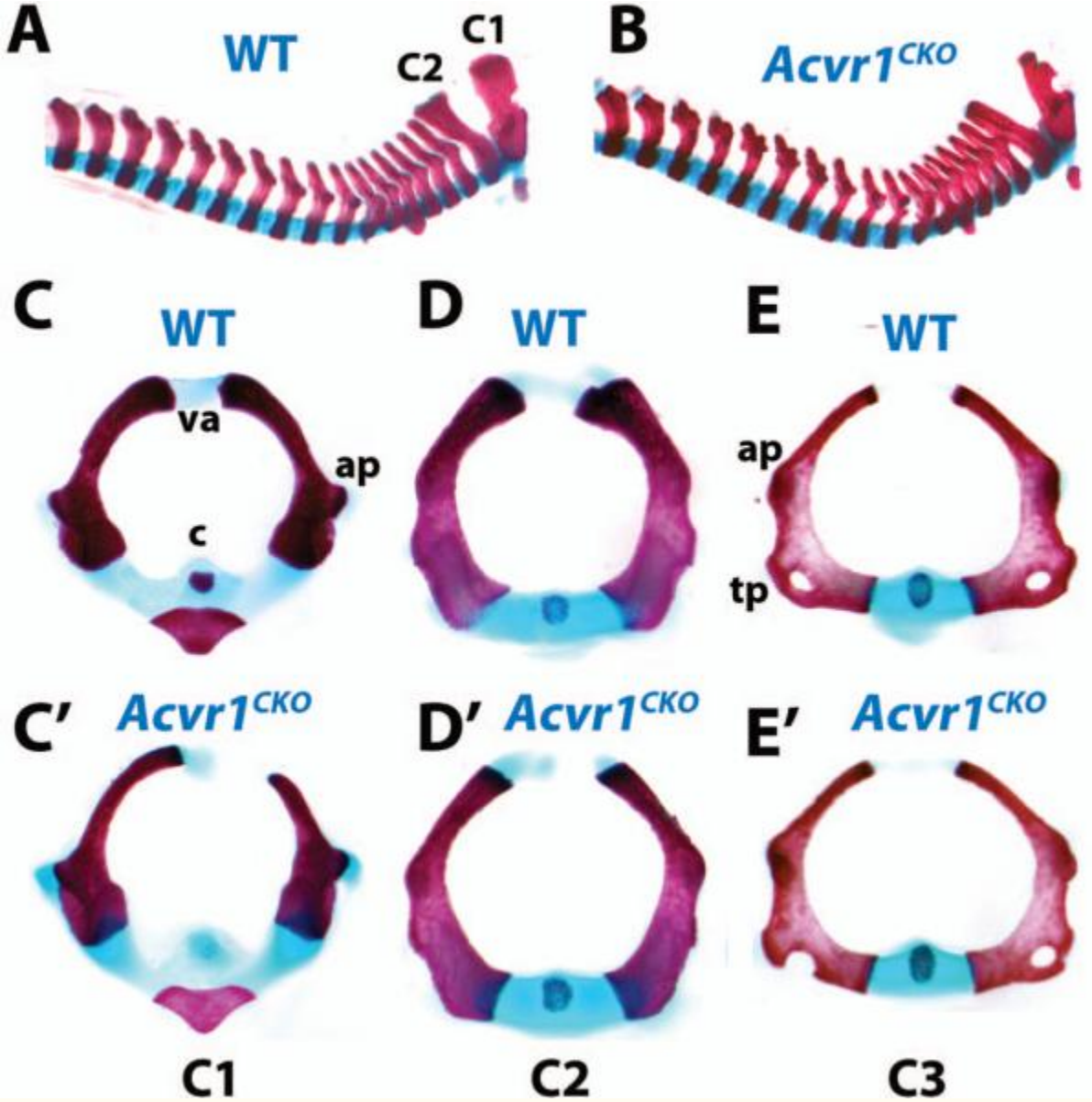

Figure 2

Axial defects in *Acvr1*$^{fx/fx}$;*Col2a1-Cre*(*Acvr1*^{CKO}) mutants

All images are whole-mount skeletal preparations of neonatal (P0) littermates stained with alcian blue/alizarin red. A, B, Cervical and thoracic spines of P0 WT (A) and *Acvr1*^{CKO} (B) littermates. C-E, transverse views of isolated WT cervical (C1-C3) vertebrae. C'-E', C1, C2, and C3 vertebrae, respectively, from *Acvr1*^{CKO} P0 littermate. ap, anterior process; c, centrum; tp, transverse process; va, vertebral arch.

BMPs exert their effects through canonical (Smad) and non-canonical (e.g., p38) pathways. Because a subtle defect was detected in *Acvr1*^{CKO} axial elements at P0 (Fig. 2), pSmad1/5/8 levels were assessed in vertebral bodies. A small but statistically significant decrease in the percentage of cells positive for pSmad1/5/8 was seen in *Acvr1*^{CKO} mutants at E17.5 (Fig. 3A,B) but not at E13.5 (data not shown). p-p38 levels were examined to determine whether differences in non-canonical BMP pathway activity could be detected. This analysis revealed an impairment in non-canonical pathway activity in mutants at E17.5 (Fig. 3C,D). Proliferation, assessed by PCNA, was indistinguishable between WT and mutant littermates at E13.5 (data not shown), but was reduced at E17.5 in *Alk2*^{CKO} vertebrae (Fig. 3E,F). Therefore, loss of ACVR1/ALK2 leads to decreased canonical and non-canonical signaling in axial chondrocytes, and this is correlated with reduced rates of cell proliferation.

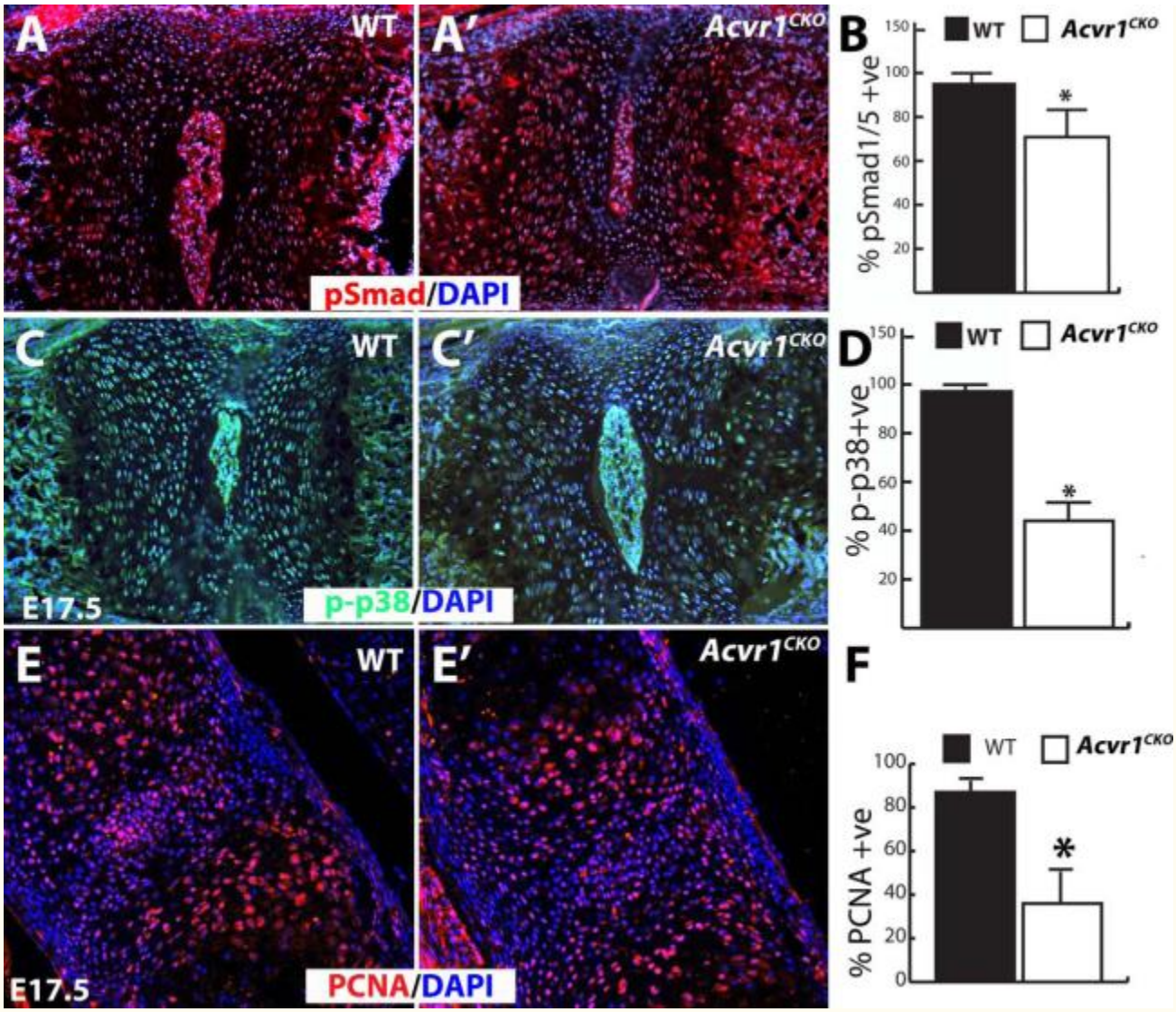

Figure 3

Impaired BMP signaling in *Acvr1$^{fx/fx}$;Col2a1-Cre*(*Acvr1^{CKO}*) mutant axial elements

All images are sagittal sections through the vertebral column of E17.5 mice counterstained with DAPI. A,A', Immunofluorescence staining for pSmad1/5 in sections through E17.5 cervical vertebrae from WT and *Acvr1^{CKO}* littermate. B, Quantitation revealed a reduction in *Acvr1^{CKO}* mice in the percentages of cells positive for pSmad1/5 compared to WT littermates (n = 16, $p < 0.0001$). C,C', Immunofluorescence staining for p-p38 in sections through E17.5 cervical vertebrae from WT and *Acvr1^{CKO}* littermate. D, Quantitation revealed a reduction in *Acvr1^{CKO}* mice in the percentages of cells positive for p-p38 compared to WT littermates (n = 9, asterisk, $p < 0.0001$). E,E', PCNA immunofluorescence on E17.5 cervical vertebrae from WT and *Acvr1^{CKO}* littermate. F, Quantitation of percentage of PCNA positive cells reveals a significant decrease in mutants. (n = 6, Asterisk, $p < 0.005$). Size differences in the nucleus pulposus for WT vs. *Acvr1^{CKO}* mice in panels A and C are not real and are a result of plane of section.

X-ray analysis of adult mice revealed no differences between WT and heterozygotes (n = 15). However, 100% of *Acvr1^{CKO}* (9/9) mice developed thoracic kyphosis (Supplemental Fig. 5A). Mutant cervical and upper thoracic vertebrae exhibited wedging characteristic of butterfly vertebrae (Supplemental Fig. 5B). Consistent with the cervical defects seen at P0 (Fig. 2), cleared skeletal preparations revealed deformations in cervical vertebrae (Supplemental Fig. 5C,D). Lumbar and sacral vertebrae were indistinguishable in adult WT and mutant littermates (data not shown). *Acvr1^{CKO}* mice also exhibited broader skulls as a result of a shortened cranial base (n = 9/9) (Supplemental Fig. 5E). Measurements of the lengths of appendicular bones revealed no differences at any stage (data not shown).

Overlapping functions with other BMP receptors

Loss of BMPR1A in cartilage leads to generalized chondrodysplasia and perinatal lethality (10). *Bmpr1b−/−* mice are viable, but exhibit appendicular skeletal defects, including brachypodism and shortened long bones (11). The pattern of ACVR1/ALK2 expression overlaps with those of BMPR1A and BMPR1B (10,26,29). Double mutants were constructed to test whether ACVR1 shares overlapping functions with these receptors.

Analysis of craniofacial (data not shown) and axial elements revealed a considerable degree of cooperative function between ACVR1 and BMPR1A. As discussed, C1 and C2 are hypoplastic in neonatal *Acvr1*^{CKO} mice (Fig. 1A,B; Fig. 4AB'; n = 6). *Bmpr1a*^{CKO} mutants also exhibited axial defects (n = 5) (Fig. 4C,C'). In contrast to *Acvr1*^{CKO} mice, where defects are most severe in cervical vertebrae, *Bmpr1a*^{CKO} mice exhibit more severe defects in thoracic vertebrae (Fig. 4B,C); vertebral arches are severely malformed in *Bmpr1a*^{CKO} (Fig. 4A'-C').

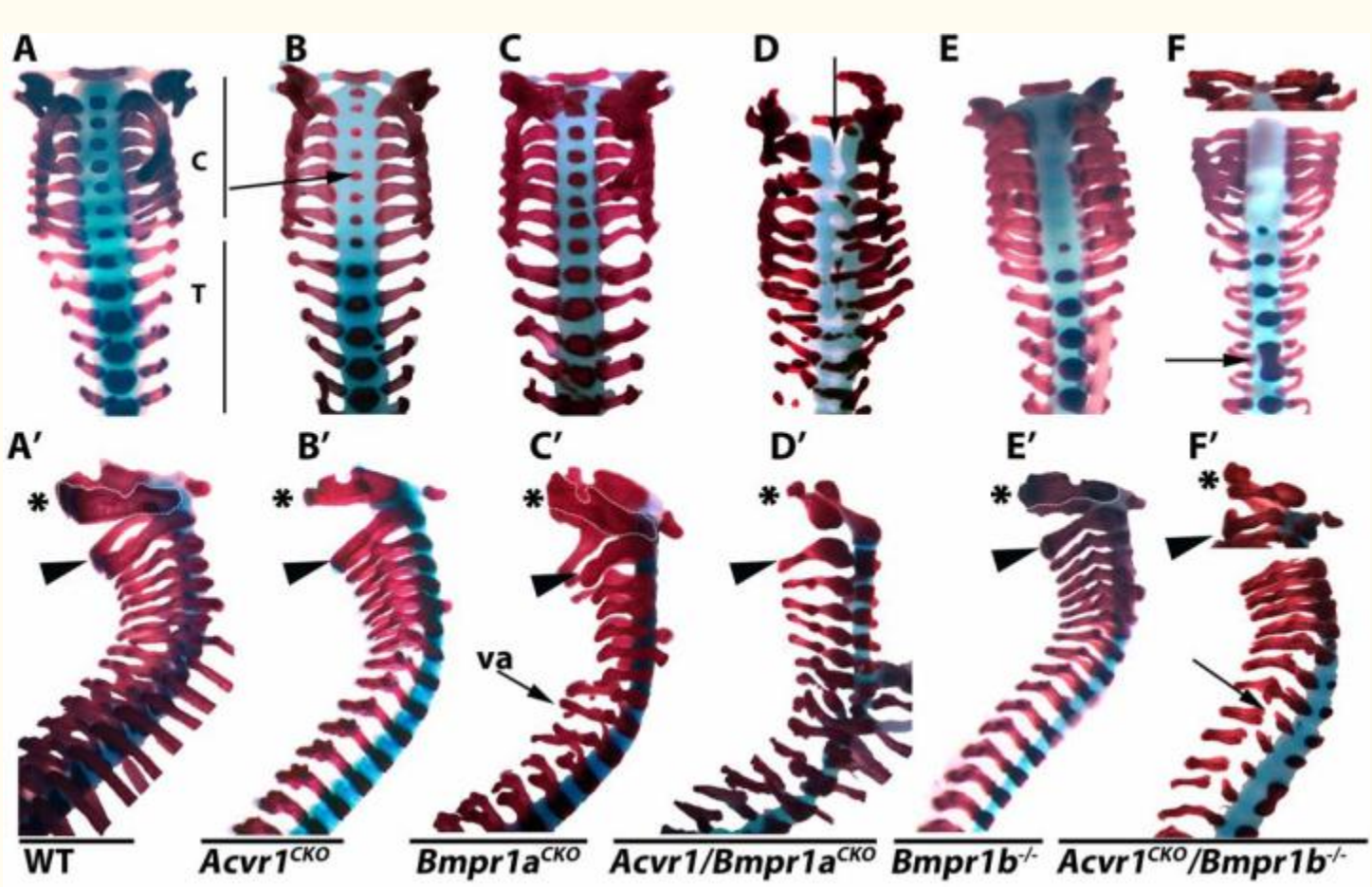

Figure 4

ACVR1/ALK2 exhibits overlapping functions with BMPR1A and BMPR1B in axial elements

All images are cleared skeletal preparations of P0 spines (disarticulated from ribs) stained with alcian blue/alizarin red. A-F, dorsal views. A'-F', lateral views. Arrow in B highlights reduced ossification of the centra in *Acvr1*^{CKO} mice. Arrow in D highlights lack of segmentation, evidenced by gaps in staining in regions where ossified centra should be located. Arrow in F highlights vertebral fusion. Arrow in F' highlights discontinuous vertebral arch. C, cervical; T, thoracic; va, vertebral arch. Asterisks in A'-F' demarcate the axis (C1). Arrowheads in A'-F' demarcate the atlas (C2).

In *Acvr1/Bmpr1a*^{CKO} double mutants, the entire vertebral column is severely malformed. Centra are absent, and the vertebral arches are diminished (Fig. 4D,D', and data not shown). In the upper cervical region,

there is a failure in segmentation (evidenced by the non-alcian blue-stained center of the spinal column (arrow in Fig. 4D). Disorganized and incomplete ossification is seen in the lower cervical and thoracic regions (Fig. 4D). At E12.5, vertebral bodies in *Acvr1/Bmpr1a*^{CKO} mutants are slightly smaller than in WT littermates, and alcian blue staining appears less intense (Supplemental Fig. 6A,B). Consistent with reduced proliferation in cervical vertebrae in E17.5 *Acvr1*^{CKO} mutants (Supplemental Fig. 3E,F), vertebral bodies appear smaller in *Alk2*^{CKO} mice at E17.5 (Supplemental Fig. 6C,D). *Acvr1/Bmpr1a*^{CKO} axial elements are disorganized (Supplemental Fig. 6C,E). There is a failure in segmentation and formation of nuclei pulposi.

Acvr1^{CKO}*/Bmpr1b−/−* P0 double mutants also exhibited craniofacial (data not shown) and vertebral abnormalities not seen in either single mutant strain. *Bmpr1b−/−* mice exhibited no ossification of the cervical centra at E17.5, but were otherwise normal (Fig. 4E,E'). This was also observed in *Acvr1*^{CKO}*/Bmpr1b* double mutants (Fig. 4F). All vertebrae were thinner than in *Bmpr1b−/−* or *Acvr1*^{CKO} mutants. Transverse processes were thin or discontinuous along the length of the vertebral column in *Acvr1/Bmpr1b* double mutants (Fig. 4F'). Vertebral fusions affecting thoracic vertebrae were occasionally observed in double mutants (n = 2/6). These were not seen in *Acvr1*^{CKO} or *Bmpr1b−/−* mice (n = 9).

As discussed, appendicular elements in *Acvr1*^{CKO} mutants were indistinguishable from those in WT littermates, except for a delay in ossification of digits (Fig. 5A,B). Forelimbs of *Bmpr1a*^{CKO} mice exhibit aplastic scapulae and shortened long bones (10) (Fig. 5C). The radius and ulna are shorter in *Acvr1/Bmpr1a*^{CKO} mice than in *Bmpr1a*^{CKO} mice (n = 6) (Fig. 5D). Similar findings were seen in hindlimbs (data not shown). Histological analysis revealed that growth plates from *Acvr1*^{CKO} mutants are indistinguishable from those of WT littermates (Fig. 5E,F). As previously shown (10), *Bmpr1a*^{CKO} growth plates exhibit disorganized and short columnar zones (Fig. 5G). In *Acvr1/Bmpr1a*^{CKO} double mutants, the columnar zone is further reduced and disorganized (Fig. 5H). ACVR1 and BMPR1B also exhibited evidence of coordinated functions in appendicular elements (Fig. 6). As shown previously, *Bmpr1b−/−* mice exhibit brachypodism accompanied by fusion and reduction of the proximal and middle phalanges, and delayed ossification of metacarpals/metatarsals (Fig. 6A,C,E,F and (11)). The reduction in ossification of the metacarpals/metatarsals is more severe in *Acvr1*^{CKO}*;Bmpr1b−/−* mutants than in either single mutant strain (Fig. 6).

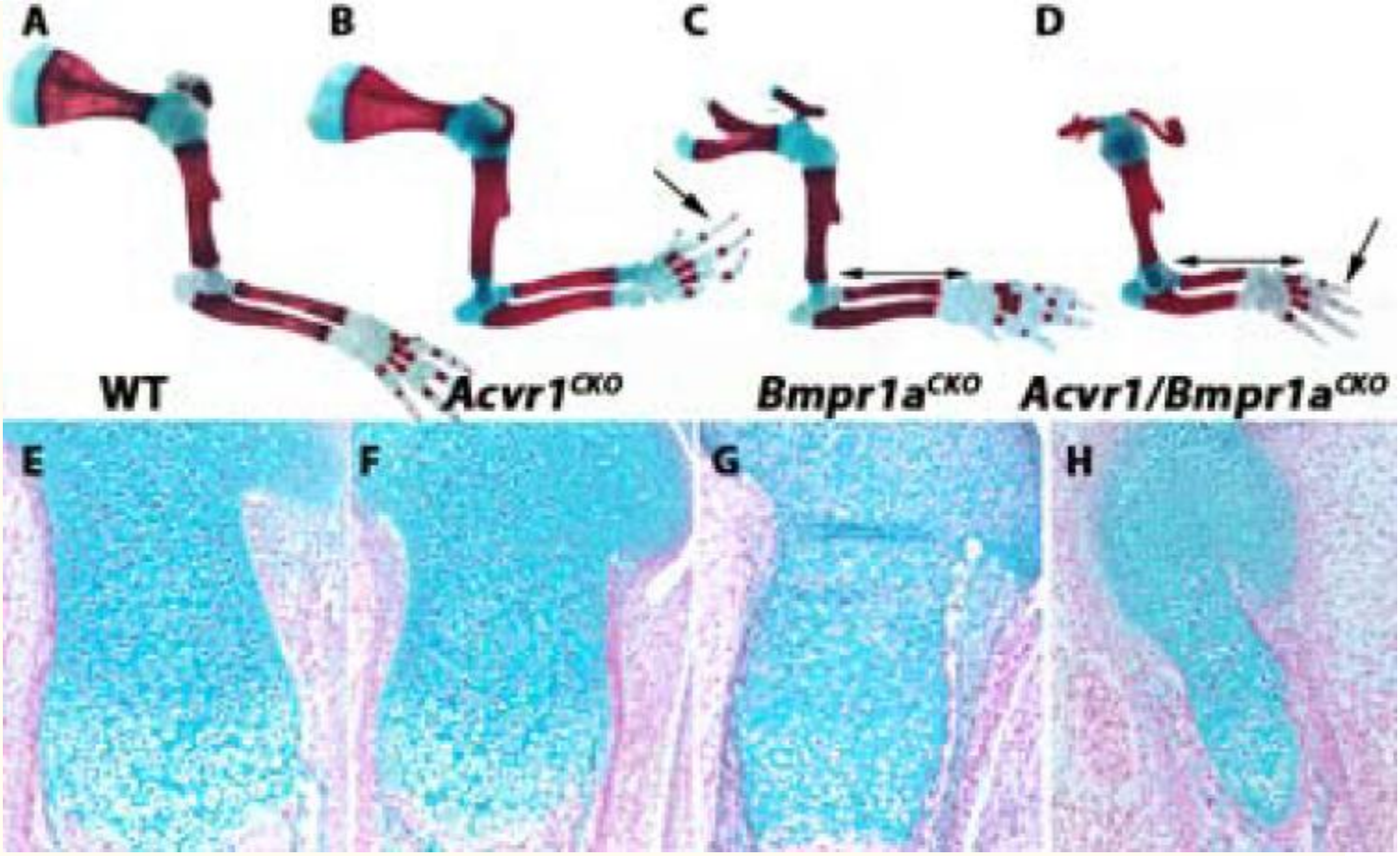

Figure 5

Appendicular defects in *Acvr1*$^{fx/fx}$;*Bmpr1a*$^{fx/fx}$;*Col2a1-Cre*(*Acvr1/Bmpr1a*^{CKO}) mice

A-D, skeletal preparations from E17.5 forearms stained with alcian blue/alizarin red. Double-headed arrows in C and D highlight shortening of radius and ulna in *Acvr1/Bmpr1a*^{CKO} mice compared to *Bmpr1a*^{CKO} mice. Arrows in B and D highlight delayed ossification of digits in *Acvr1*^{CKO} mice, which is exacerbated in *Acvr1/Bmpr1a*^{CKO} mice. E-H, sagittal sections through proximal femurs of E17.5 mice of the indicated genotypes stained with alcian blue/nuclear fast red.

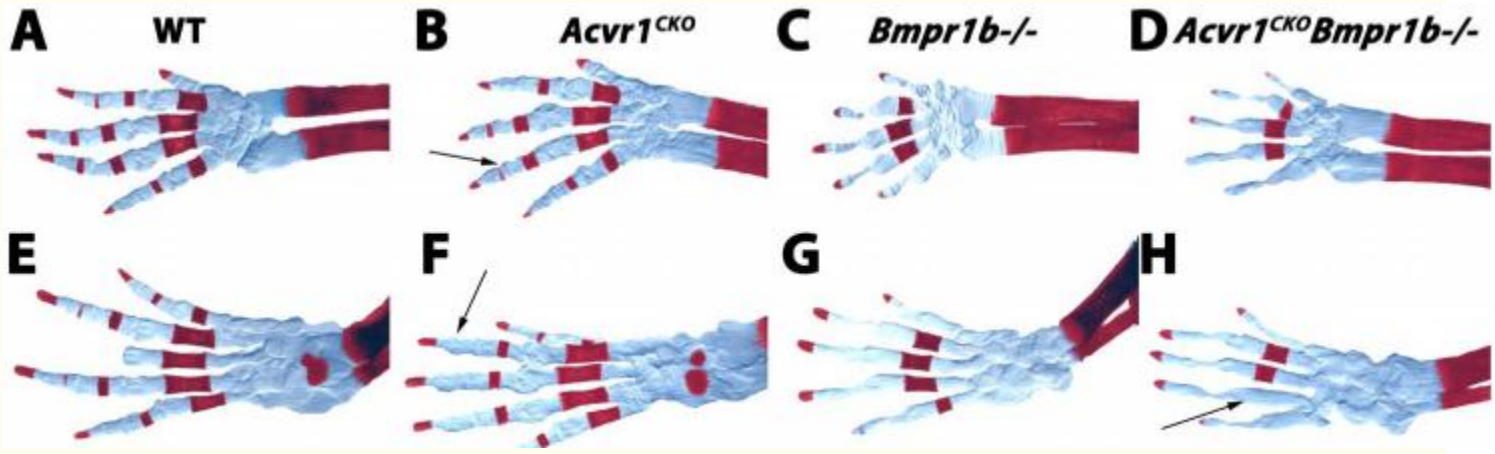

Figure 6

Appendicular defects in *Acvr1*$^{fx/fx}$;*Bmpr1b*−/−;*Col2a1-Cre* (*Acvr1*^{CKO}/*Bmpr1b*−/−) mice

Cleared skeletal preparations from E17.5 autopods of forelimbs (A-D) and hindlimbs (E-H) stained with alcian blue/nuclear fast red. A blue filter was applied in Photoshop to the images to enhance visualization of alcian blue-

stained regions. Arrows in B and F point to reduced or absent ossification in phalangeal elements in *Acvr1*^{CKO} mice. Arrow in H highlights absence of ossification in the *Acvr1*^{CKO}*/Bmprb−/−* hindlimb compared to the *Acvr1*^{CKO} and *Bmpr1b−/−* single mutant strains.

Discussion

These studies demonstrate that ACVR1/ALK2 is essential for normal endochondral bone formation. Mice lacking *Bmpr1a* in cartilage exhibit lethal chondrodysplasia (6). Loss of *Bmpr1b* in mice and humans is not lethal, and defects are most prominent in appendicular elements (11,30,31). We show here that *Acvr1*^{CKO} mice are viable but exhibit craniofacial and axial defects. Thus, BMPR1A appears to have global functions, whereas ACVR1/ALK2 and BMPR1B have more restricted roles in committed chondrocytes in axial and appendicular elements, respectively. These differential roles may reflect differences in expression of these receptors or the BMP ligands that activate them (11).

All three type I receptors are expressed to some extent in appendicular, axial, and craniofacial elements, raising the possibility of overlapping or coordinated functions. This was shown for BMPR1A and BMPR1B by the absence of cartilage in *Bmpr1a*^{CKO}*;Bmpr1b−/−* mice (6). Here we show that ACVR1 also exerts overlapping functions in committed chondrocytes with BMPR1A and BMPR1B. Combined loss of ACVR1 and either BMPR1A or BMPR1B leads to perinatal lethality and generalized chondrodysplasia.

Fibrodysplasia ossificans progressiva (FOP) patients harbor an activating mutation in *Acvr1* (15,16). However, there are few developmental effects of this activating mutation in cartilage, the most penetrant of which is malformation of the great toes. This has also been demonstrated in chimeric mice carrying the FOP mutation (32). Although delayed ossification of digits was observed in *Acvr1*^{CKO} mice, there were no additional defects in the great toe. It is important to bear in mind, however, that in *Acvr1*^{CKO} mice, excision occurs only in committed chondrocytes. Therefore limb patterning defects that might affect the great toe would not be expected. Some FOP patients exhibit congenital abnormalities in the cervical spine, the area most severely affected in *Acvr1*^{CKO} mice. In FOP patients, the cervical spine exhibits large spinous processes and progressive fusion of articular processes (33,34). In *Acvr1*^{CKO} mice, cervical spinous and articular processes are hypoplastic. Thus, cervical vertebrae are sensitive to both gain and loss of ACVR1 function. The basis for the strong effects of ACVR1 on cervical elements in relation to other vertebrae is unclear, but might be related to the fact that cervical vertebrae are the earliest to be specified in mammals but the last to become ossified, thus requiring a longer period of growth and development (35,36).

We show here that loss of ACVR1 also leads to craniofacial defects. Distinct facial defects have been reported in a subset of FOP patients, including a reduced mandible and underdevelopment of the supra-orbital ridge (37). Defective mandibular development was reported in mice lacking ACVR1 in cranial neural crest cells (21). Distinct craniofacial defects were observed in the present study, which can be attributed to defects in chondrogenesis in the cranial base. It is thus conceivable that some of the facial features seen in FOP patients are a consequence of altered development of the cranial base. Similarly, conductive hearing loss is seen in about 50% of FOP patients (34). It is conceivable that this is due to craniofacial defects affecting the inner ear.

We did not detect obvious changes in appendicular elements in *Acvr1*^{CKO} mice. However, proximal medial tibial osteochondromas and short broad femoral necks are common but variable features of FOP patients (34). We cannot rule out the possibility that there are subtle defects in appendicular elements in *Acvr1*^{CKO} mice. The fact that the appendicular skeletons of both *Acvr1/Bmpr1a*^{CKO} and *Acvr1*^{CKO}*/Bmpr1b−/−* mice are more severely affected than those of *Bmpr1a*^{CKO} or *Bmpr1b−/−* mice demonstrates that ACVR1 is expressed in and plays a role in the development of appendicular elements.

The precise mechanisms by which ACVR1 exerts its effects during chondrogenesis are unknown. We found that loss of ACVR1 led to reduced canonical (pSmad1/5) and non-canonical (p-p38) activity in axial elements, as has also been seen in mice lacking BMPR1A and/or BMPR1B in cartilage (10,11). The majority of the literature has focused on the ability of ACVR1 to activate canonical Smads 1/5/8. This has been demonstrated most clearly using constitutively active or FOP variants of ACVR1 (16,21). Our observation of a reduction in pSmad1/5 levels in *Acvr1*^{CKO} mutants is consistent with these findings. ACVR1/ALK2 can activate non-canonical pathways in addition to canonical ones. For example, it was reported that ACVR1 regulates cell proliferation during formation of the vertebrate lens in a Smad-independent manner (38). Thus, the reduced p-p38 levels in *Acvr1*^{CKO} mutants may contribute to the observed chondrocyte proliferation defects. These are not mutually exclusive possibilities. Regardless of the precise mechanism, the strong synergy in phenotype seen in *Acvr1/Bmpr1a*^{CKO} and *Acvr1*^{CKO}*/Bmpr1b*$-/-$ double mutants strongly argues that ACVR1 exerts its effects through BMP signaling pathways.

The fact that *Acvr1/Bmpr1a*^{CKO} double mutants exhibit defects along the entire length of the spine indicates that ACVR1 and BMPR1A have coordinated functions in all axial elements. The *Acvr1/Bmpr1a*^{CKO} phenotype resembles that of *Pax1/9* double mutants, in which failure of sclerotomal cells to migrate ventrally leads to the loss of medial structures such as the centra (39). This is consistent with the fact that *Col2a1-Cre* is expressed in the sclerotome (19). The observation that rates of proliferation are reduced in committed chondrocytes in vertebral elements in *Acvr1*^{CKO} mice indicates that ALK2 plays a role at multiple stages of chondrogenesis.

The subtlety of the developmental limb phenotype in *Acvr1*^{CKO} mice can be attributed at least in part to overlapping functions with both BMPR1A and BMPR1B. It is also possible that the *Acvr1* limb phenotype is less severe than the axial one because *Col2a1-Cre* is first expressed in committed chondrocytes in appendicular elements (19). It is conceivable that ACVR1 also has important functions in the limb at an earlier stage; studies utilizing *Prx1-Cre* would be very informative in this regard, although as discussed above, we (Fig. 1, Supplemental Fig. 2) and others (26) did not detect high levels of ACVR1 expression in prechondrogenic condensations in the limb. Similarly, it is possible that ACVR1 plays a role in maintenance of articular cartilage. Although ACVR1 does not appear to be as highly expressed as BMPR1A or BMPR1B in articular cartilage (40), extra-articular ankylosis of all major joints is a key feature of FOP (41). Post-natal ablation of ACVR1 in cartilage would be required to address this question and to separate direct effects on articular cartilage from indirect effects resulting from abnormal development.

Finally, we show that ACVR1 is strongly expressed in the notochord and nucleus pulposus, raising the possibility that this receptor plays an essential role in the formation/maintenance of these structures. ACVR1 has been shown to regulate the rate of cell proliferation in the node, the transient embryonic structure that gives rise to the notochord (42). The use of a notochord-specific Cre line will be required to address the function, if any, of ACVR1 in the notochord and its derivatives.

In summary, this study shows that all three type I BMP receptors play essential roles in committed chondrocytes. BMPR1A appears to have the most prominent function, as *Bmpr1a*^{CKO} mutants exhibit generalized chondrodysplasia, while defects in *Bmpr1b*$-/-$ mice are seen primarily in appendicular elements, whereas those in *Acvr1*^{CKO} mice are primarily found in axial and craniofacial elements. The extent to which ACVR1 transduces its signals in cartilage through the canonical Smad pathway vs. non-canonical pathways is unknown; we show that loss of ACVR1 impacts levels of both canonical pSmads and noncanonical p-p38. However, we have shown previously that BMPs transduce the majority of their signals in committed chondrocytes through R-Smad pathways, and we have shown here genetically that ACVR1 exerts overlapping functions with BMPR1A and BMPR1B. These findings suggest that ACVR1 also

transduces its effects in cartilage to a significant extent through R-Smad-mediated pathways, but future studies are needed to address this issue.